ELSEVIER

Journal of Nuclear Materials 276 (2000) 143–153

journal of nuclear materials

www.elsevier.nl/locate/jnucmat

Computer simulation of fundamental behaviors of interstitial clusters in Fe and Ni

E. Kuramoto*

Research Institute for Applied Mechanics, Kyushu University, 6-1 Kasuga-koen, Kasuga-shi, 816-8580, Japan

Abstract

Atomistic features of small interstitial clusters in Fe and Ni have been investigated by computer simulation. The gradual change from an interstitial cluster to a dislocation loop was observed in detail from three points of view, (i) strain distribution along crowdion axis for each crowdion in a cluster, (ii) distribution of Burgers vector of peripheral dislocation line of a cluster, and (iii) recombination behavior of a vacancy of with a cluster. It is found that strain distribution was spread into two opposite directions on a crowdion axis with the increase of a cluster size. The irregularity on the curve of the distribution of Burgers vector of a smaller loop gradually disappears with the increase of a loop size. Recombination between a crowdion and a vacancy occurs on the peripheral position of smaller clusters, but this does not occur in larger clusters. These aspects show that the gradual change from an interstitial cluster to a dislocation loop occurs at a certain width of cluster size. Dynamic behavior was also investigated under cylindrical shear stress and the Peierls stress was obtained as a function of loop size. The results show that the Peierls stress decreases with increasing loop size down to the value of a straight edge dislocation. Activation energies of one atomic jump of these small dislocation loops were also calculated and small values of about 0.2 eV were found for loops of about 200 crowdions for both Fe and Ni.

1. Introduction

In materials under irradiation environments the defect cluster formation process plays an important role for the damage structure generation because it is closely related to the production of the imbalance between vacancy and interstitial fluxes during irradiation, namely, the so-called bias factor. Many theoretical attempts have been performed to understand the bias phenomena, such as dislocation bias [1–5], production bias [6,7] and so on. However, fundamental properties of the defect clusters have not been clearly understood yet, especially the atomic structure of the small clusters and their interaction behavior with other crystalline defects, such as dislocations. A better understanding of the whole damage generation process, void swelling, radiation embrittlement and so on necessitates more investigations. In the present study attempts will be made to clarify the atomistic features of small interstitial clusters and their behavior under applied shear stress in model Fe and Ni lattices, which are typical bcc and fcc metals and are important elements in ferritic and austenitic stainless steels, respectively. Especially the difference between small interstitial clusters and dislocation loops will be investigated in detail.

Clusters of crowdions will be mainly investigated in detail because these clusters have possibility of dynamic response, that is, gliding along the direction of crowdion axis. It is accepted that the increase of a cluster size causes gradual change from a small interstitial cluster to a dislocation loop. To understand this gradual change three attempts will be made to clarify the elemental process, that is, (i) to observe the change of the strain distribution along crowdion axis for each crowdion in a cluster. (ii) to observe the distribution of Burgers vector of peripheral dislocation line of a cluster, and (iii) to observe the recombination behavior with a vacancy of each crowdion on a peripheral position of a cluster.

* Tel: +81-92 583 7766; fax: +81-92 583 7767.

E-mail address: kuramoto@himiko.riam.kyushu-u.ac.jp (E. Kuramoto)

0022-3115/00/$ - see front matter
PII: S0022-3115(99)00174-9

2. Method of calculation

Computer simulation of the behavior of small interstitial clusters with N-body potentials like EAM type potential was made. The potentials given by Finnis and Sinclair [8,9] and by Gao et al. [10] were used for Fe and Ni, respectively. Interstitial clusters were introduced into the central region of the model lattices shown in Fig. 1(a) and (b) for Fe and Ni, respectively. Sizes of the model lattices are $60b \times 60(2/3)^{1/2}b \times 60(2 \cdot 2^{1/2}/3)b$ and $60b \times 60(2/3)^{1/2}b \times 60(3^{1/2}/2)b$ (b: magnitude of Burgers vector) for Fe and Ni, respectively as shown in Fig. 1, where the orientation of the model lattices are also shown. Whole lattice with a defect cluster was fully relaxed by the static method (Newton–Raphson method) under the fixed boundary condition. This static method has no temperature effect, then all the results obtained correspond to $T = 0$ K. The size of the model lattice was chosen as large as possible to avoid the boundary effect. Small interstitial clusters are constructed by making bundles of crowdions on low index atomic planes, $\langle 1\,1\,1 \rangle$ crowdions on $\{1\,1\,0\}$ or $\{1\,1\,1\}$ atomic planes (loop planes) in Fe and $\langle 1\,1\,0 \rangle$ crowdions on $\{1\,1\,1\}$ or $\{1\,1\,0\}$ atomic planes (loop planes) in Ni.

3. Results and discussion

3.1. Cluster size effect on the strain distribution on a crowdion axis in interstitial clusters

The strain field around a single crowdion is one dimensionally spreading towards two opposite directions along its axis. The direction of crowdion axis is along $\langle 1\,1\,1 \rangle$ and $\langle 1\,1\,0 \rangle$ atomic rows for Fe and Ni, respectively. It must be investigated how this situation might be changed when crowdions form a cluster. In Fig. 2 the atomic structure of a typical interstitial cluster, a bundle of 19 crowdions I_{19} in Fe is shown from two different directions to the loop, top view (a) and front view (b). In Fig. 2(b) the structure of bundled crowdions are clearly seen.

In Fig. 3 the strain distribution along a $\langle 1\,1\,1 \rangle$ crowdian axis in interstitial clusters, $(a/2)\ \langle 1\,1\,1 \rangle$ dislocation loops is shown for Fe as a function of cluster size compared with that of a straight edge dislocation. The abscissa Z is the atomic position on a $\langle 1\,1\,1 \rangle$ crowdion axis in unit of b (magnitude of Burgers vector, interatomic distance along $\langle 1\,1\,1 \rangle$ direction in a perfect lattice) and the ordinate $Z_{k+1} - Z_k - 1$ (b unit) is the interatomic distance between two adjacent atoms on a crowdion axis – b. All negative values in the figure show

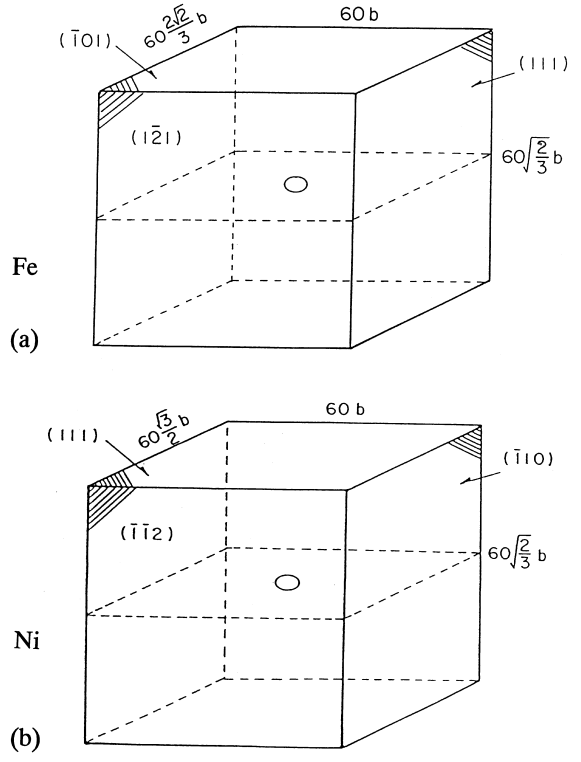

Fig. 1. Model lattice for (a) Fe and (b) Ni for the construction of interstitial clusters.

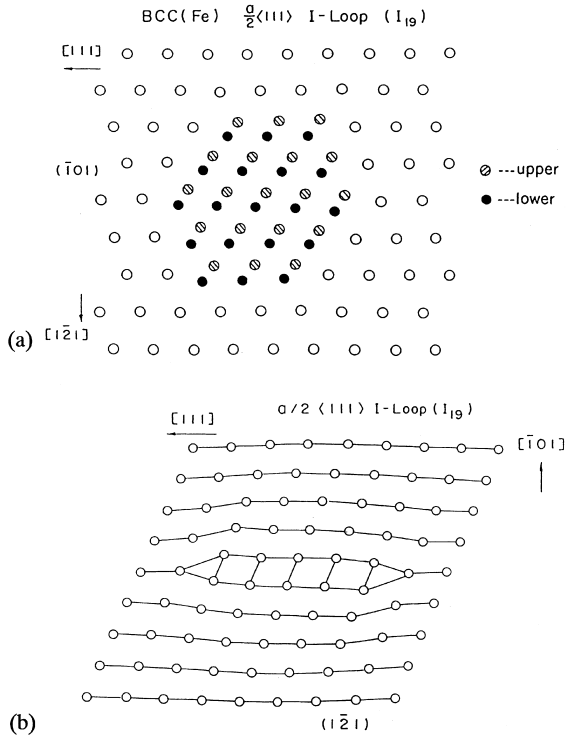

Fig. 2. Atomic configuration of an intersititial cluster I_{19}, $(a/2)$ $\langle 1\,1\,1 \rangle$ dislocation loop in Fe, (a) top view and (b) front view.

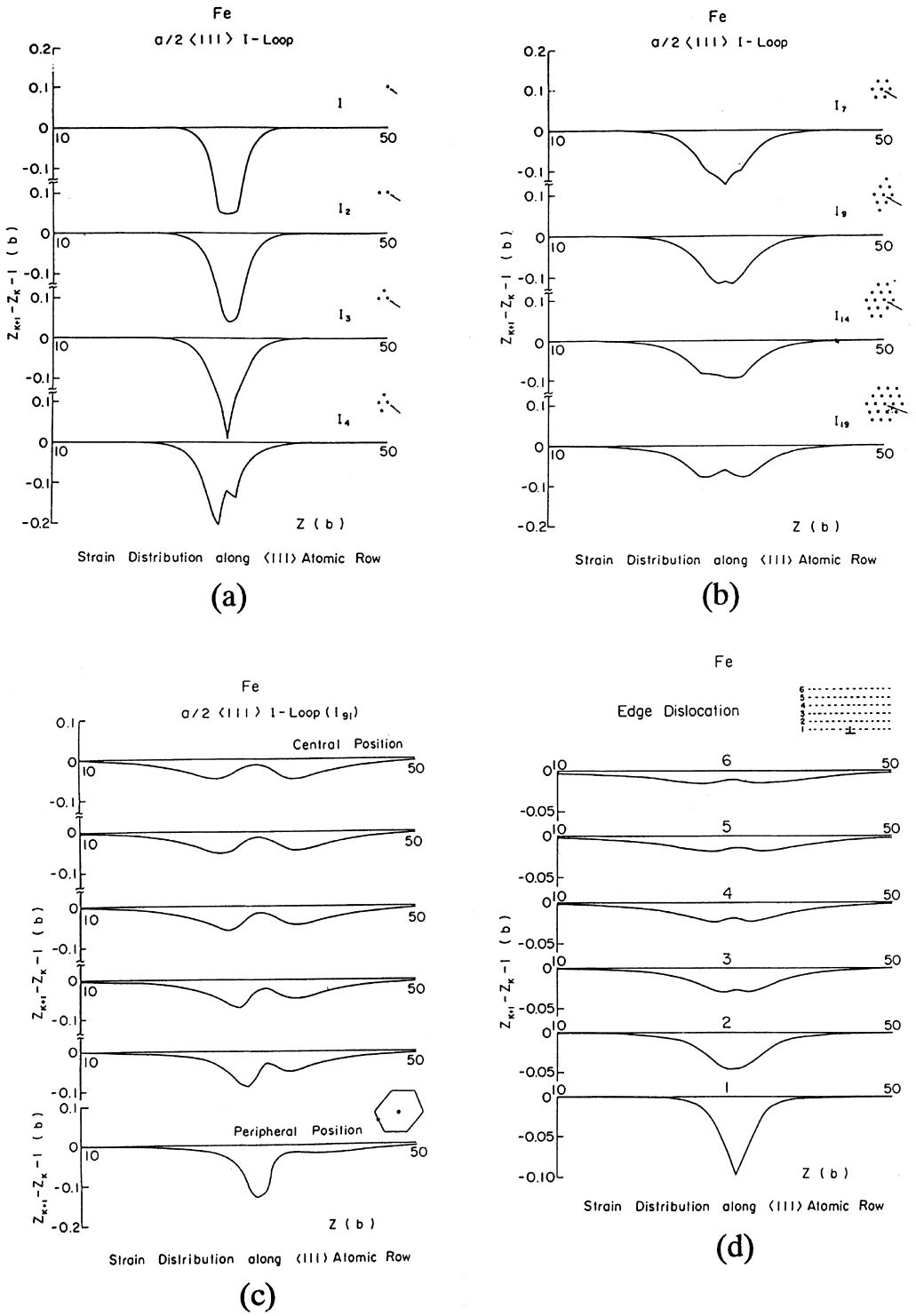

Fig. 3. Distribution of the interatomic distance between two adjacent atoms on a ⟨1 1 1⟩ crowdion axis in interstitial clusters in Fe: the abscissa Z is the atomic positon on a ⟨1 1 1⟩ crowdion axis in unit of b (magnitude of Burgers vector) and the ordinate $Z_{k+1} - Z_k - 1$ (b unit) is the interatomic distance between two adjacent atoms on the crowdion axis – b. Results are shown for $I - I_4$ (a), for $I_7 - I_{19}$ (b), for I_{91} (atomic rows at central to peripheral positions) (c), and for a straight edge dislocation (d). The atomic row on which the interatomic distance was measured is shown by a small arrow in the symbolic mark of interstitial clusters drawn beside.

that the interatomic distances are shorter than b. In the figure the atomic row on which the interatomic distance was measured is shown by a small arrow in the symbolic mark of interstitial clusters drawn beside. The case of $I_1 - I_4$ is shown in Fig. 3(a), that of $I_7 - I_{19}$ in Fig. 3(b), that of I_{19} (atomic rows located at central to peripheral positions) in Fig. 3(c), and that of a straight edge dislocation in Fig. 3(d).

It is realized that the localized strain of an isolated crowdion becomes split gradually into two parts in opposite sides with increasing cluster size. This splitting tendency is more prominent at the central part of a cluster, but at a peripheral position of a large loop this splitting does not occur as shown in Fig. 3(c). The splitting of strain observed here shows that the structure change to a perfect lattice takes place especially from the central part of a cluster.

This tendency is also observed for the case of a straight edge dislocation shown in Fig. 3(d), where the same splitting occurs on the $\langle 1\,1\,1 \rangle$ atomic rows parallel to the Burgers vector with increasing distance from the slip plane. On the slip plane this splitting does not occur just like the case of peripheral position in Fig. 3(c), which corresponds to the fact that a dislocation in Fe is not extended, but is a perfect dislocation. The similarity between clusters and an edge dislocation suggests that the interstitial clusters tend to a dislocation loop with increasing cluster size.

Results of the same kind of calculation made for an interstitial cluster I_{91}, $(a/2)\,\langle 1\,1\,0 \rangle$ dislocation loop and an edge dislocation in Ni are shown in Fig. 4. In Ni the extended character of a straight edge dislocation is much more pronounced because of the low stacking fault energy. Corresponding to this fact, the extension occurs even in the dislocation loop, namely, among six segments of a hexagonal-shaped loop four segments on $\{1\,1\,1\}$ atomic planes are extended, but the other two segments on $\{1\,0\,0\}$ atomic planes are not extended. Distributions of the interatomic distance on a $\langle 1\,1\,0 \rangle$ crowdion axis shown in Fig. 4(a) are corresponding to

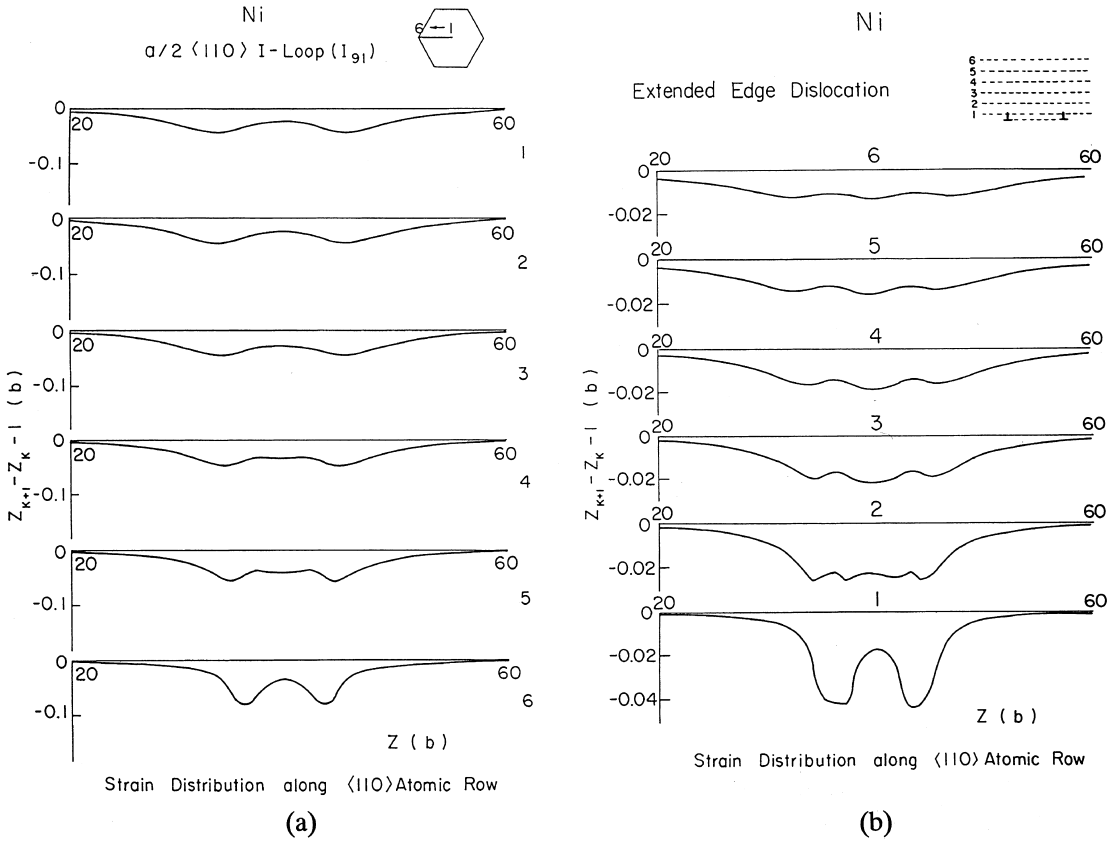

Fig. 4. Distribution of the interatomic distance between two adjacent atoms on each $\langle 1\,1\,0 \rangle$ crowdion axis in an interstitial cluster I_{91} in Ni: the abscissa Z is the atomic positon on a $\langle 1\,1\,0 \rangle$ crowdion axis in unit of b (magnitude of Burgers vector) and the ordinate $Z_{k+1} - Z_k - 1$ (b unit) is the interatomic distance between two adjacent atoms on the crowdion axis – b. Result for I_{91} is shown in (a), that for a straight extended edge dislocation in (b). Numbers in the figure correspnds to the $\langle 1\,1\,0 \rangle$ atomic rows on which the interatomic distancetance was measured.

the ⟨1 1 0⟩ atomic rows 1–6 from the central position to the peripheral position denoted in the figure. The atomic row 6 is located in the extended part of the dislocation loop, then the distribution is already split as shown in the figure. The atomic row 1 (central position) shows rather spread strain distribution than the atomic row 6 (peripheral position). As shown in Fig. 4(b) in the case of a straight extended edge dislocation in Ni the same splitting occurs on the ⟨1 1 0⟩ atomic rows parallel to the Burgers vector, and the strain is spreading with increasing distance from the slip plane. Similarity between an interstitial cluster and an edge dislocation is again observed in the case of Ni as well as Fe. Namely, this similarity is clearly seen in I_{91} both in Fe and Ni, but the tendency of strain splitting already started to appear in smaller clusters like I_{19}.

3.2. Burgers vector of dislocation loops

In Fig. 5 the distribution of Burgers vector of the dislocation line of a loop, i.e., the peripheral line of a cluster is plotted for the case of I_{61}, an interstitial cluster of 61 crowdions and also for a straight edge dislocation for Fe. Here the distribution of Burgers vector $\rho_b(x)$ (b unit) in the ordinate is defined by the differential displacement $\mathrm{d}u(x)/\mathrm{d}x$ ($u(x)$ is the displacement shown above in the figure in unit of b) between two adjacent {1 1 0} atomic planes just above and below the slip plane of a dislocation segment of a hexagonal-shaped loop. The value of $u(x)$ changes from zero to one (b unit) on the x axis (vertical to the dislocation line, in unit of b) in the range $-\infty \sim +\infty$ along the slip plane. The slip plane is a surface of a hexagonal-shaped tube which is in

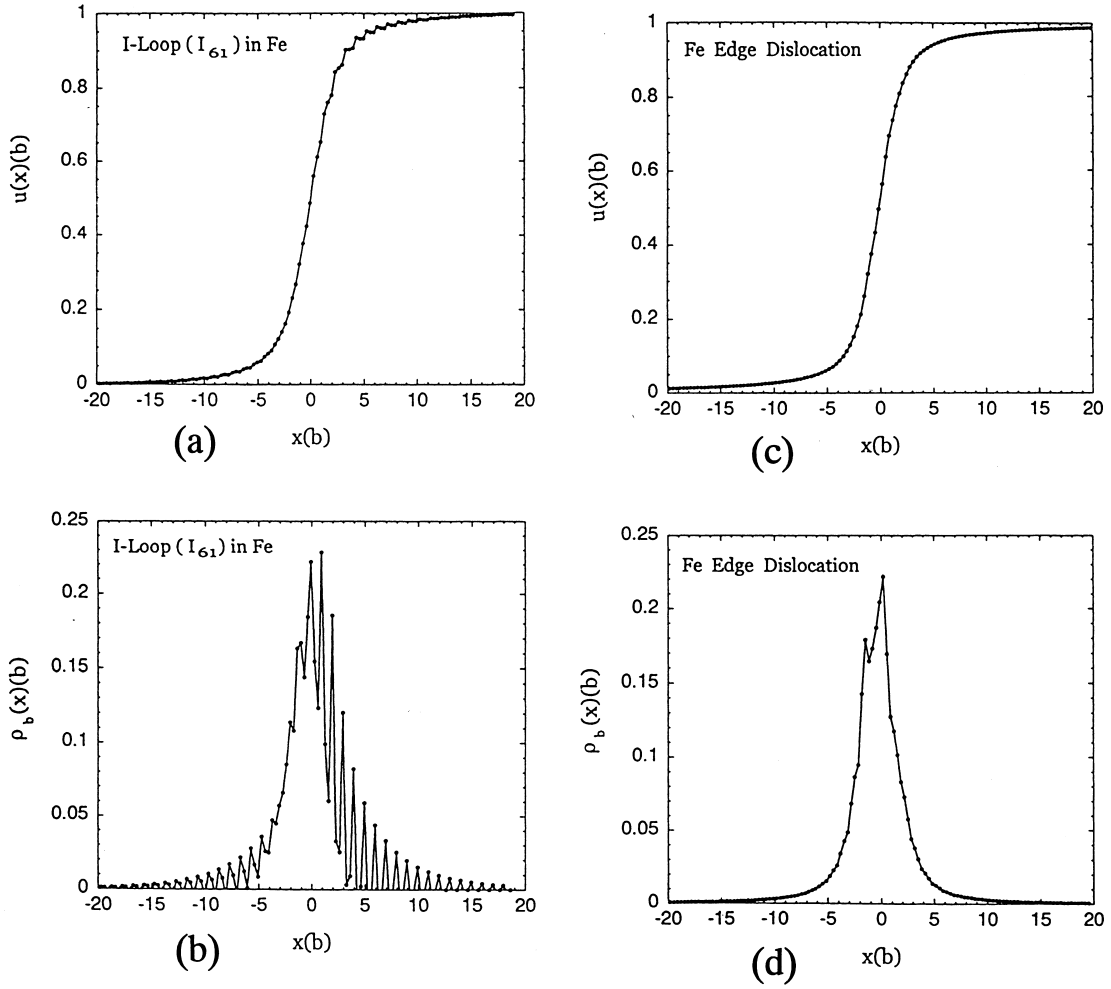

Fig. 5. Distribution of Burgers vector of an interstitial cluster of 61 crowdions, I_{61} ($(a/2)$ ⟨1 1 1⟩ dislocation loop), compared with that of a straight edge dislocation in Fe: $\rho_b(x)$(b unit) in the ordinate is defined by the differential displacement $\mathrm{d}u(x)/\mathrm{d}x$ ($u(x)$ is the displacement shown above in the figure in unit of b) between two adjacent {1 1 0} atomic planes just above and below the slip plane of a dislocation segment of a hexagonal-shaped loop.

contact with a hexagonal-shaped loop and consists of six {1 1 0} planes.

It is seen from Fig. 5 that the irregularity exists on the distribution curves of Burgers vector $\rho_b(x)$ for an interstitial clusters of 61 crowdions, I_{61} ($(a/2)$ ⟨1 1 1⟩ dislocation loop), but gradually disappears with the increase of a loop size (the irregularity is less in I_{217}) and a dislocation loop approaches to a perfect edge dislocation line. This irregularity is considered to be caused by a loose core structure of a dislocation loop compared with a straight edge dislocation. In other word, each crowdion in a cluster still possesses its own character, resulting in the irregularity of the Burgers vector curve.

3.3. Recombination with a vacancy

Another way to clarify the basic mechanism of the gradual transition from a small interstitial cluster, i.e., a bundle of crowdions to a dislocation loop is to investigate the interaction behavior with a trial vacancy put on the core region, because this must be tightly related to the looseness of the core of a dislocation loop.

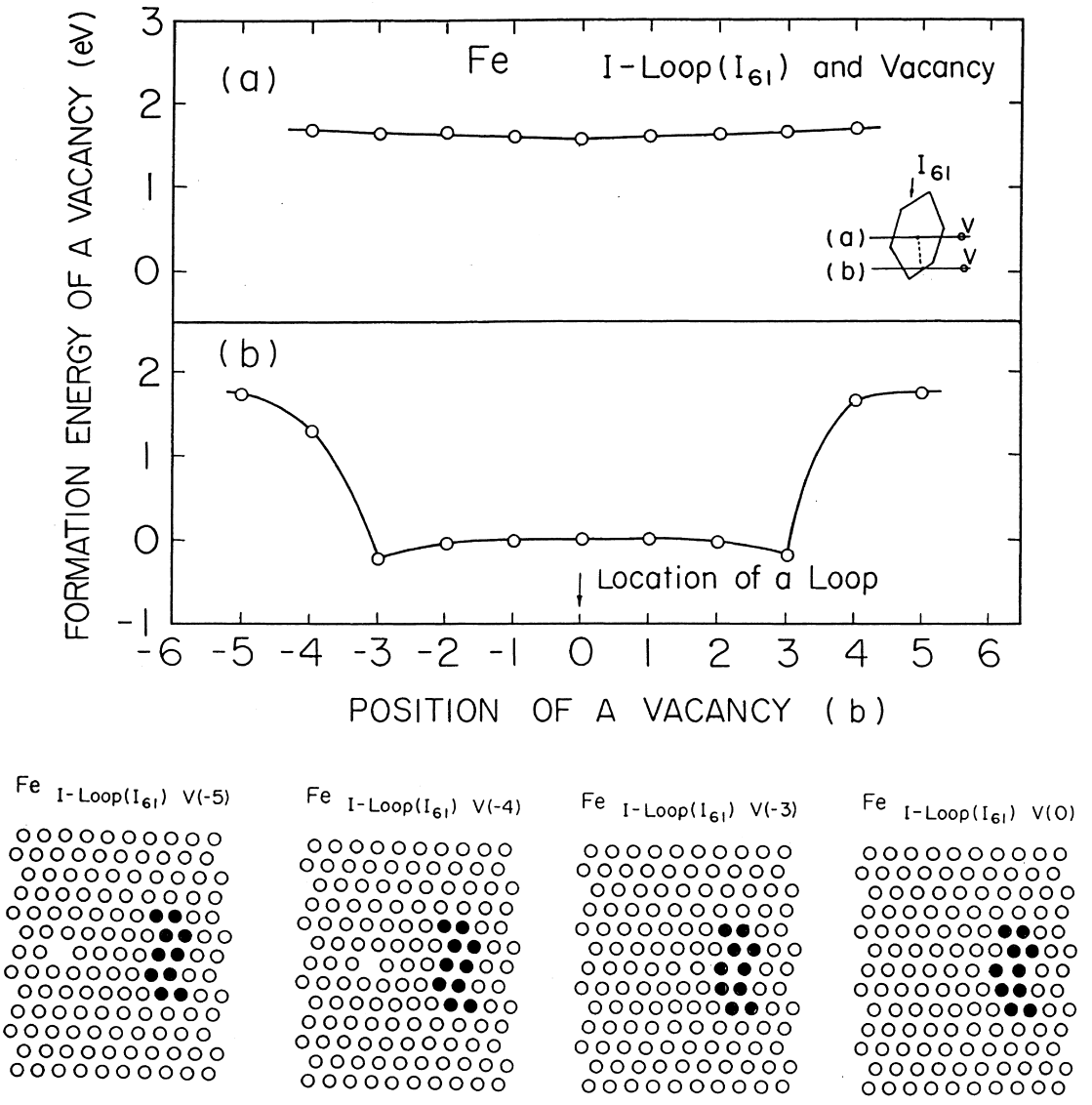

Fig. 6. Change of vacancy formation energy as a function of a distance from the core of a dislocation loop I_{61} in Fe (direction of ⟨1 1 1⟩ crowdion axis, parallel to Brugers vector on the {1 1 0} slip plane) and actual atomic configurations on {1 1 0} atomic plane on which a vacancy exists.

In Figs. 6 and 7 calculated vacancy formation energies are plotted as a function of the distance from the dislocation core, namely, along ⟨1 1 1⟩ crowdion axis, the direction of Burgers vector. In case (b) in the figure a vacancy was placed on the line through the dislocation core, namely, the peripheral position of the loop as shown schematically in the figure, but in case (a) a vacancy was placed on the line penetrating the center of a loop. Vacancy formation energy was obtained by the conventional method, that is, (total energy of a crystal with a vacancy + I-cluster)−(total energy of a crystal without a vacancy + I-cluster + E_c (cohesive energy per atom)).

As a vacancy approaches to the core of a dislocation loop the formation energy starts to decrease at a few atomic distances from the core of a dislocation loop, that is, from 1.83 eV at the distant region to almost zero at the core region for the case of I_{61} in Fe as shown in Fig. 6 (curve (b)). Corresponding atomic configurations on horizontal {1 1 0} atomic plane are also shown below

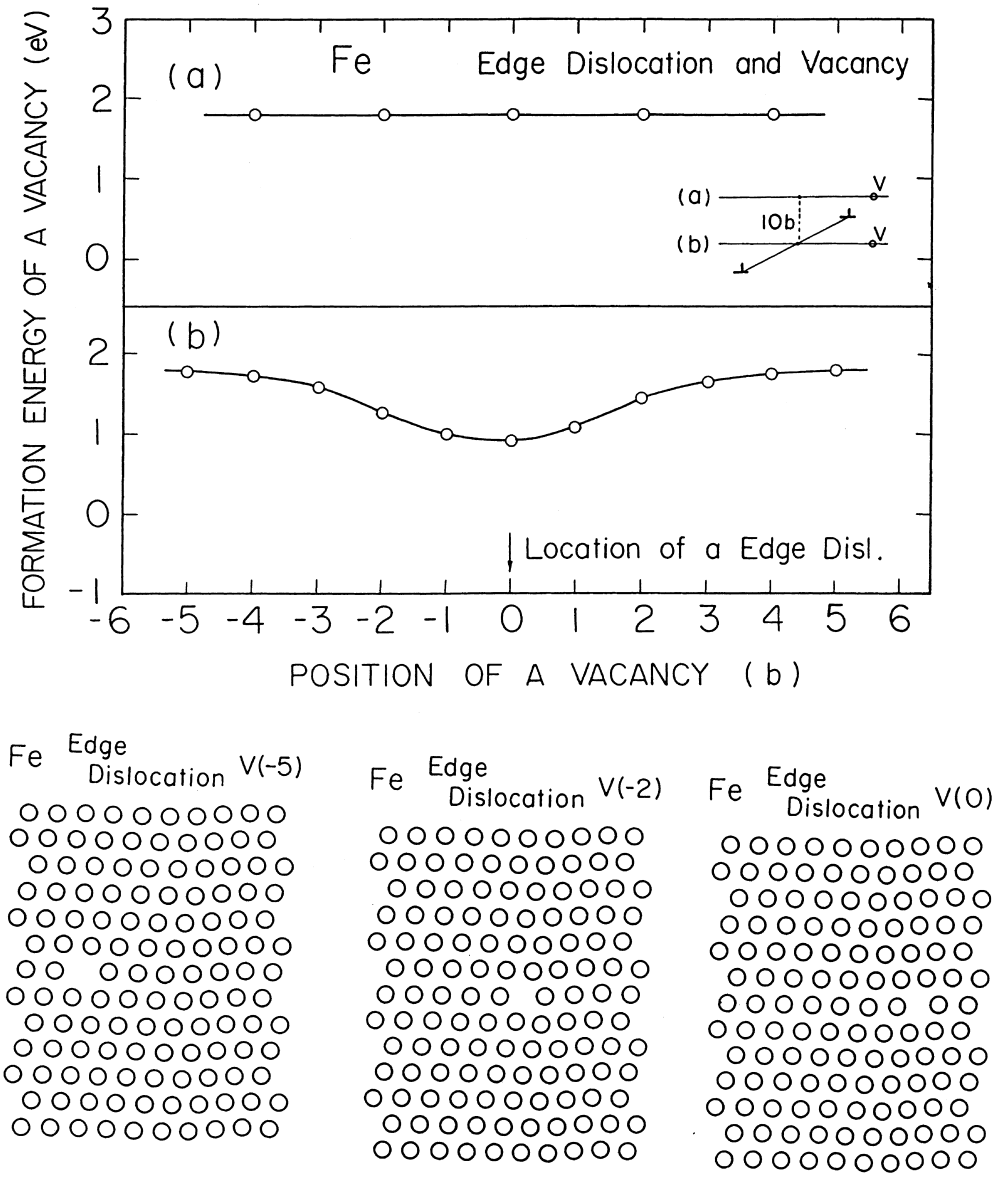

Fig. 7. Change of vacancy formation energy as a function of a distance from the core of a straight edge dislocation in Fe (direction of ⟨1 1 1⟩ crowdion axis, parallel to Brugers vector on the {1 1 0} slip plane) and actual atomic configurations on {1 1 0} atomic plane on which a vacancy exists.

in Fig. 6. It is seen that a vacancy is collapsed at the core region (marked dark), that is, recombination occurs completely at the core region as shown in the right two figures (V(−3) and V(0), number is a position of a vacancy in unit of b), but in the left two figures (V(−5) and V(−4)) vacancies are left uncollapsed without complete recombination, and with high formation energies. In other words, in the former a dislocation loop I_{61} recombines with a vacancy and is changed into I_{60} , which has a jog on the dislocation line, but in the latter they are left as a dislocation loop I_{61} and a vacancy. As seen from the curve (a) in the figure nothing occurs along the central line ($\langle 1\,1\,1\rangle$ direction) of a loop I_{61} when a vacancy is placed, suggesting that this part of a loop already has a property of a perfect crystal.

The same procedure was performed also for the interaction between a vacancy and a straight edge dislocation in Fe as shown in Fig. 7. In this case the vacancy formation energy decreases from 1.83 eV (at a distant region) to 0.9 eV (at a dislocation core), but not to zero observed in the case of the dislocation loop shown in Fig. 6. From the atomic configurations on $\{1\,1\,0\}$ atomic plane drawn below in Fig. 7 it is clearly known that recombination is not completed, that is, a vacancy still has a free volume even at the dislocation core region shown in V(0) as well as V(−2) and V(−5). This situation must be considered to be a vacancy trapped at the dislocation core, not a jog. This means that in the case of a straight edge dislocation the character of a crowdion completely disappears, confirmed by the incomplete recombination behavior with a vacancy. In other word, the core structure of a straight edge dislocation is very tight, and the property of each crowdion is not maintained.

3.4. Dynamical behavior of dislocation loops under applied shear stress

The response to the applied shear stress, namely, dynamic behavior of the dislocation loops was also investigated by applying the axially symmetrical shear stress on a dislocation loop as shown in Fig. 8, where a model Fe lattice of a size of 80 $b\times 80\ (2/3)^{2/3}\ b\times 40\ (2\cdot E2^{1/2}/3)\ b$ with a dislocation loop at the center is shown. Since a straight dislocation makes a glide motion under the shear stress applied on the slip plane, each segment of a hexagonal-shaped dislocation loop can also make a glide motion under the shear stress applied on each slip plane, namely, applied equally on the six $\{1\,1\,0\}$ slip planes of a hexagonal tube which is in contact with a loop. This is the reason why the axially symmetrical shear stress was chosen in Fig. 8.

The motion of the dislocation loop under the axially symmetrical shear stress was oberved by relaxing the whole lattice fully by the static method (Newton–Raphson method) under the fixed boundary condition.

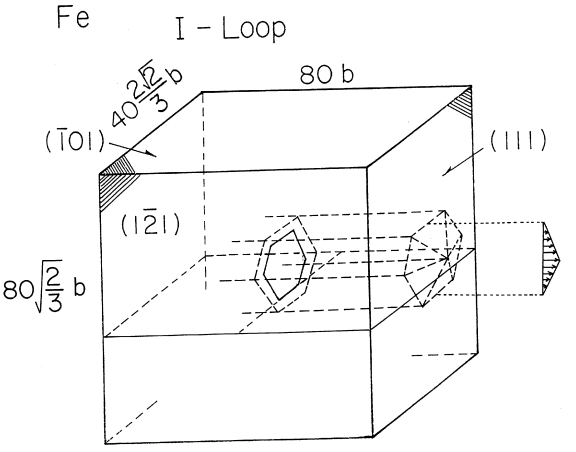

Fig. 8. Application of the axially symmetrical shear stress on a dislocation loop $(a/2)\ \langle 1\,1\,1\rangle$ dislocation loop in a model Fe lattice.

This static method has no temperature effect, then all the results obtained correspond to $T = 0$ K. This process was repeated with increasing the applied shear stress stepwise. The position of the dislocation loop was determined by measuring the Burgers vector dislocation mentioned above after each step of stressing. The central position of the Burgers vector distribution thus obtained gives the present position of the dislocation loop. Beyond a certain value of this applied shear stress the dislocation loop started to move, and the corresponding distance over which the dislocation loop moved around $b/4$.

The stress necessary to move a dislocation loop is considered to be Peierls stress for the loop. It was made clear that this Peierls stress (the stress to move a loop to $b/4$) has a decreasing tendency as increasing of a loop size (I_{19}, I_{61}, $\{1\,1\,1\}$ loop plane for Fe, and I_{61}, I_{127}, I_{217}, $\{1\,1\,0\}$ loop plane for Ni) and approaches to the level of that of a straight edge dislocation as shown in Figs. 9 and 10 for Fe and Ni, respectively. Absolute values of Peierls stress is larger for Fe than Ni, which corresponds to the result of yield stress measurement.

To understand this decreasing tendency the core structure of a dislocation loop was drawn as shown in Figs. 11 and 12 as a function of loop size with that of a straight edge dislocation for Fe and Ni, respectively. Arrows in the figure denote the differential displacements between two atomic planes just above and below the slip plane. In the core region arrows have large magnitude due to large strain around a core region, and in the distant region they show vanishing tendency, because the crystal comes back to a perfect lattice. From these figures it is recognized that the extension of the core decreases with decreasing loop size. It is known that the localized core usually gives higher Peierls stress,

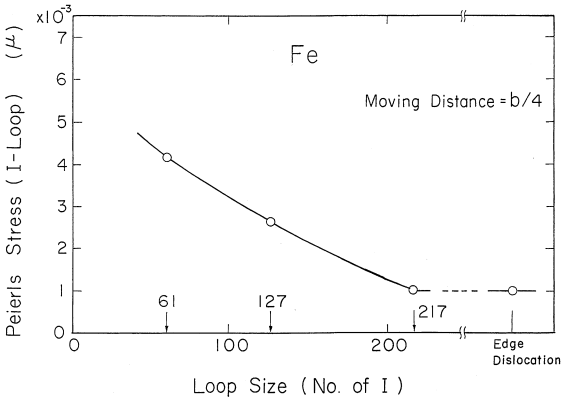

Fig. 9. Relation between the Peierls stress (the stress to move a loop to $b/4$, in unit of shear modlus μ) for $a/2\langle 111\rangle$ dislocation loop and loop size, i.e., number of $\langle 111\rangle$ crowdions in a dislocation loop for Fe.

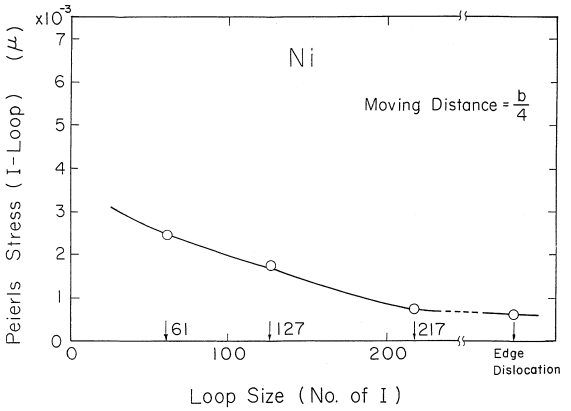

Fig. 10. Relation between the Peierls stress (the stress to move a loop to $b/4$, in unit of shear modulus) for $a/2\langle 110\rangle$ dislocation loop and loop size, i.e., number of $\langle 110\rangle$ crowdions in a dislocation loop for Ni.

which is able to explain the decreasing tendency of Peierls stress obtained in the present simulation.

3.5. Activation energy for a motion of dislocation loop

The activation energy required for overcoming the Peierls barrier for the motion of a dislocation loop was calculated by integrating the force–distance curve, namely, τbl–d curve obtained from the result of stepwise stressing a dislocation loop. Here τ is the shear stress applied on the dislocation loop, τb is the force acting on the unit length of a loop, l is a total length of circumference of a loop, d is a distance moved. The schematic drawing is shown in Fig. 13, where twice of the shadowed area corresponds to the peak height of the potential. In Figs. 14 and 15 the obtained activation

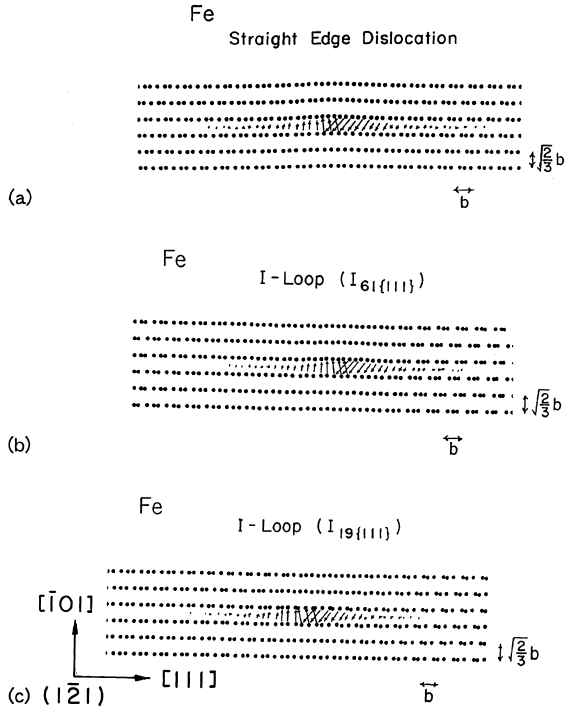

Fig. 11. Core structure of dislocation loops and a straight edge dislocation in Fe: Arrows in the figure denote the differential displacements between two atomic planes just above and below the slip plane, showing larger magnitude in the core region and vanishing tendency in the distant region (coming back to a perfect lattice).

energies for Fe and Ni are shown as a function of loop size, respectively, where increasing tendency is seen with increasing loop size. On the other hand, the limit of the smallest loop must be a crowdion itself. The migration energy of the self-interstitial atom is reported as 0.3 eV for Fe and 0.15 eV for Ni (these values are corresponding to stage I in the recovery of the electrical resistivity after low temperature irradiation [11]. It is usually recognized that the stage I corresponds to the migration of dumbbell type interstitial atom, then the migration energy of a crowdion might be less than this value. Recent calculation by Soneda and Diaz de la Rubia [12] found that the migration energy of a single SIA in Fe is of 0.16 eV. Hence the curve in this figure might increase in the smallest loop size limit as shown by a dotted line. The value of action energy is about 0.2 eV at a loop of about 200 interstitial atoms, which is very small and might be thermally activated easily at high temperatures. This is consistent with the reported observation of motion of small interstitial clusters in the electron microscope [13]. The activation energy increases with increasing loop size because force includes the length of circumference of a loop. It is considered that for a large enough loop a kink pair formation might

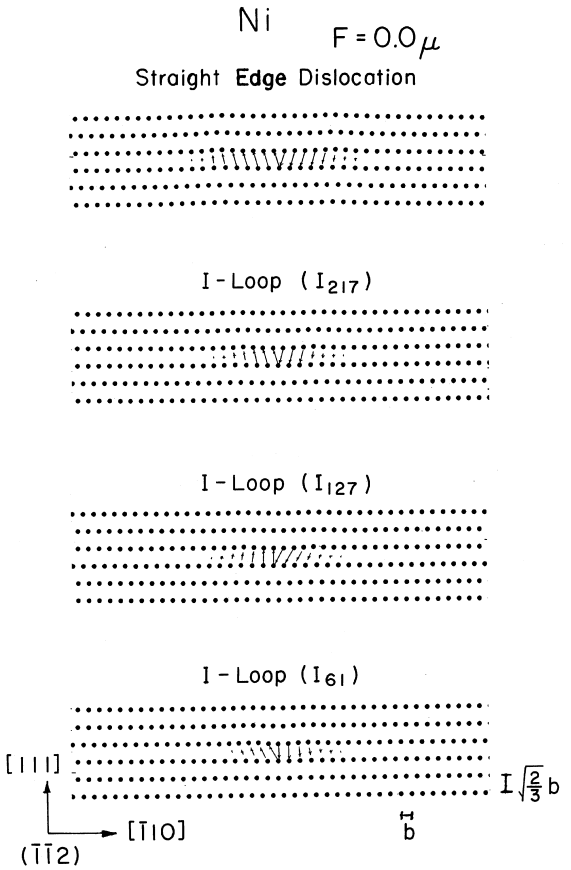

Fig. 12. Core structure of dislocation loops and a straight edge dislocation in Ni: Arrows in the figure denote the differential displacements between two atomic planes just above and below the slip plane, showing larger magnitude in the core region and vanishing tendency in the distant region (coming back to a perfect lattice).

occur just like a straight dislocation, then the increasing tendency will cease automatically.

4. Conclusion

To understand the gradual change from an interstitial cluster to a dislocation loop three attempts have been made. Clusters of self-interstitial atoms (crowdions) in Fe and Ni were formed in the model lattice and it was found that as the number of crowdions in a cluster increases, splitting of the localized strain occurs along the crowdion axis especially in the central part of a loop. This effect suggests that clusters have tendency to convert to dislocation loops. Distribution of Burgers vector was also investigated and irregularity is observed in a smaller loop, but with the increase of loop size this irregularity disappears. Recombination behavior with a

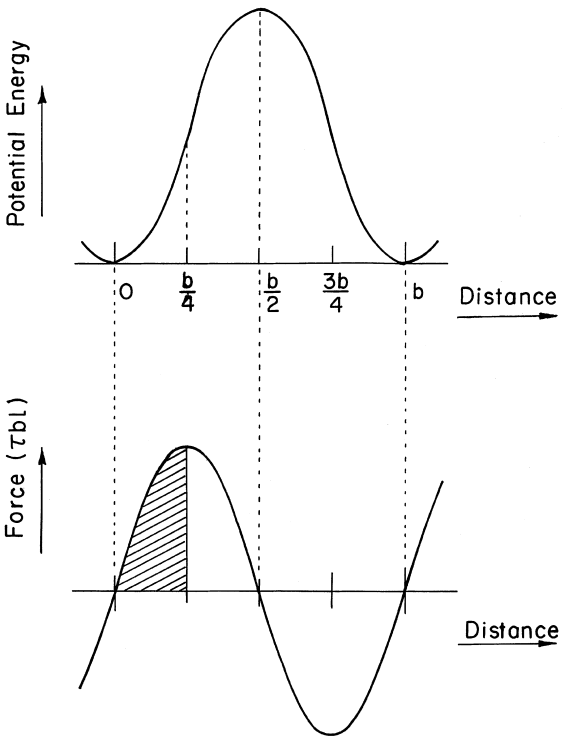

Fig. 13. Schematic drawing of force–distance curve (τbl–d curve) for a motion of a dislocation loop: t is the shear stress applied on the dislocation loop, τb is the force acting on the unit length of a loop, l is a total length of circumference of a loop, d is a distance moved.

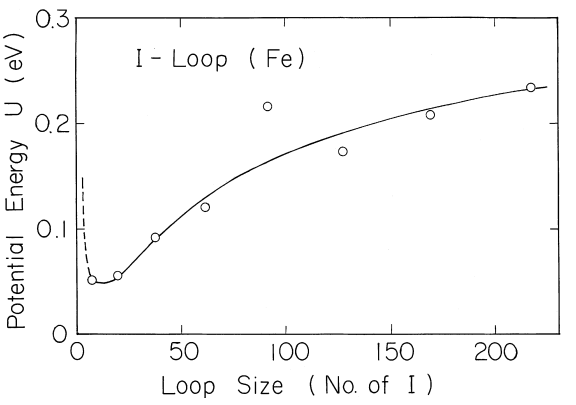

Fig. 14. Calculated activation energy for a motion of a dislocation loop as a function of loop size (number of interstitial atoms in a loop) in Fe.

vacancy was studied and it was found that in smaller loops recombination between a crowdion from the peripheral position of a loop and a vacancy occurs, but in larger loops this does not, similar to the case of straight edge dislocation. These aspects show that, if its size is

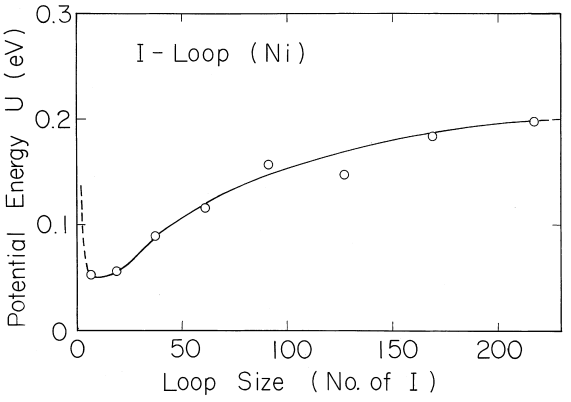

Fig. 15. Calculated activation energy for a motion of a dislocation loop as a function of loop size (number of interstitial atoms in a loop) in Ni.

bigger than about 200 (number of crowdions in a cluster) for both Fe and Ni, an interstitial cluster behaves like a dislocation loop. But this gradually changing tendency to a dislocation loop already occurred even at smaller clusters. Dynamic behavior of a dislocation loop was investigated under the axially symmetrical shear stress. It was found that Peierls stress for a dislocation loop decreases as the loop size increases due to the extension of core region of a dislocation loop. Activation energies of one atomic jump of these small dislocation loops were also calculated and small values of about 0.2 eV was found for loops of about 200 crowdions for both Fe and Ni.

References

[1] R. Bullough, B.L. Eyre, K. Krishan, Proc. Roy. Soc., London, A346 (1975) 81.
[2] P.T. Heald, Philos. Mag. 35 (1975) 551.
[3] E. Kuramoto, J. Nucl. Mater. 179–181 (1991) 1019.
[4] E. Kuramoto, J. Nucl. Mater. 191–194 (1992) 1279.
[5] E. Kuramoto, T. Tustusmi, J. Nucl. Mater. 212–215 (1994) 175.
[6] C.H. Woo, B.N. Singh, Philos. Mag. A 65 (1992) 889.
[7] T. Diaz de la Rubia, M.W. Guinan, Phys. Rev. Lett. 66 (1991) 2766.
[8] M.W. Finnis, J.E. Sinclair, Philos. Mag. A 50 (1984) 45.
[9] M.W. Finnis, J.E. Sinclair, Philos. Mag. A 53 (1986) 161 (erratum to Ref. [8]).
[10] F. Gao, D.J. Bacon, G.J. Ackland, Philos. Mag. A 67 (1993) 275.
[11] H.J. Wollenberger, Physical Metallurgy, in: R.W. Cahn, P. Haasen (Eds.), North Holland Physics, Amsterdam, 1983, p. 1189.
[12] N. Soneda, T. Diaz de la Rubia, Philos. Mag. A 78 (1998) 995.
[13] M. Kiritani, J. Nucl. Mater. 206 (1993) 156.